

samples (from 2- and 10-m depth) for DIC, Alk, and $\delta^{13}\text{C}$ at Station S, located 26 km southeast of the island of Bermuda (32°10'N, 64°30'W) (27). In 1989, the Joint Global Ocean Flux Study BATS program was established at a station 56 km further southeast (31°50'N, 64°10'W) (38). The CDRG program extended their measurements to this new site, and the BBSR started to measure DIC there throughout the water column (24). Because differences between Station S and BATS have been found to be small (38), and because the DIC data from the two laboratories show no systematic differences (change in DIC = $-1.0 \pm 2.2 \mu\text{mol kg}^{-1}$, $N = 78$ measurements), the data from the two sites and two laboratories are combined here into a single time series.

20. The reduced isotopic ratio, $\delta^{13}\text{C}$, is defined as $\delta^{13}\text{C} = (R_{\text{sample}}/R_{\text{std}} - 1) \times 1000$, where R_{sample} is the $^{13}\text{C}/^{12}\text{C}$ ratio of the sample, and where R_{std} is the $^{13}\text{C}/^{12}\text{C}$ ratio of the Pee Dee belemnite standard.

21. We computed the oceanic $p\text{CO}_2$ from the observed temperature, salinity, Alk, DIC, and nutrients using a thermodynamic model of the carbonate system (39) and the dissociation constants of Mehrbach *et al.* (40) as refitted by Dickson and Millero (41). This choice is based on laboratory studies (42) and the resulting good agreement with direct observations of $p\text{CO}_2$ near Bermuda (43).

22. R. B. Bacastow, C. D. Keeling, T. J. Lueker, M. Wahlen, W. G. Mook, *Global Biogeochem. Cycles* **10**, 335 (1996).

23. N. Gruber *et al.*, *Global Biogeochem. Cycles* **13**, 307 (1999).

24. N. R. Bates, *Deep-Sea Res. II* **48**, 1507 (2001).

25. This trend is smaller than that reported by Bates (24) for 1988 to 1998, mainly because of smaller growth rates in the 1980s.

26. R. E. Sonnerup *et al.*, *Global Biogeochem. Cycles* **13**, 857 (1999).

27. C. D. Keeling, in *The Global Carbon Cycle*, M. Heimann, Ed. (Springer-Verlag, New York, 1993), pp. 413–430.

28. T. M. Joyce, P. Robbins, *J. Clim.* **9**, 3121 (1996).

29. N. Gruber, C. D. Keeling, T. F. Stocker, *Deep-Sea Res. I* **45**, 673 (1998).

30. Net community production refers to the net transfer between inorganic and organic carbon pools due to photosynthesis and to oxidation of organic matter, and therefore is equal to net primary production minus community respiration.

31. Materials and methods are available as supporting material on Science Online.

32. Because the time-series sites are located in the broad recirculation region of the subtropical North Atlantic, the geostrophic mean currents are from the northeast. Current meter data indicate a mean current of about 0.05 m s^{-1} (44), although substantially higher velocities are associated with the passage of eddies. Based on the observed mean horizontal gradient near Bermuda of about $1.1 \times 10^{-5} \mu\text{mol kg}^{-1} \text{ m}^{-1}$ (29), our model-derived transport estimates give horizontal velocities of between -0.01 and -0.20 m s^{-1} , with a long-term mean of -0.07 m s^{-1} (negative velocity indicates southward flow).

33. The uncertainties of the fluxes have been established with a Monte Carlo technique (45). The diagnostic model was run 1000 times, with randomly selected sets of parameter values within a predetermined range for each parameter based on the parameter's perceived uncertainty (29). The flux uncertainties listed in the text denote the $1-\sigma$ uncertainty computed from the results of these 1000 realizations.

34. Because our diagnostic model analyses cannot uniquely determine the underlying mechanisms, other factors, such as variations in mesoscale eddy dynamics, or dust deposition and its possible impact on N_2 fixation, could be responsible for our positive correlation of net community production with winter mixed-layer depth anomalies.

35. R. L. Molinari, D. A. Mayer, J. F. Festa, H. F. Bezdek, *J. Geophys. Res.* **102**, 3267 (1997).

36. N. R. Bates, A. C. Pequignot, R. J. Johnson, N. Gruber, *Nature* **420**, 489 (2002).

37. The atmospheric CO_2 inversion results have been provided by P. Bousquet and P. Peylin and are based

on the anomalous CO_2 fluxes for the entire North Atlantic region as estimated in their global study (4).

38. A. F. Michaels, A. H. Knap, *Deep-Sea Res. II* **43**, 157 (1996).

39. U.S. Department of Energy, "Handbook of methods for the analysis of the various parameters of the carbon dioxide system in sea water," version 2, *Tech. Rep. ORNL/CDIAC-74* (U.S. Department of Energy, Carbon Dioxide Information Analysis Center, Oak Ridge National Laboratory, Oak Ridge, TN, 1994).

40. C. Mehrbach, C. H. Culberson, J. E. Hawley, R. M. Pytkowicz, *Limnol. Oceanogr.* **18**, 897 (1973).

41. A. G. Dickson, F. J. Millero, *Deep-Sea Res.* **34**, 1733 (1987).

42. T. J. Lueker, A. G. Dickson, C. D. Keeling, *Mar. Chem.* **70**, 105 (2000).

43. N. R. Bates, T. Takahashi, D. W. Chipman, A. H. Knap, *J. Geophys. Res.* **103**, 15567 (1998).

44. D. A. Siegel, W. G. Deuser, *Deep-Sea Res. I* **44**, 1519 (1997).

45. R. Y. Rubinstein, *Simulation and the Monte Carlo Method* (Wiley, New York, 1981).

46. T. J. Conway *et al.*, *J. Geophys. Res.* **99**, 22831 (1994).

47. We are grateful to the numerous people who have been responsible for the collection, preparation, and analysis of the data presented here. We thank in particular P. Guenther, T. Lueker, G. Emanuele, E. Bollenbacher, and A. Dickson at the Scripps Institution of Oceanography. We also thank A. Knap, A. Michaels, D. Steinberg, C. Carlson, and D. Hansell for their help and support. We are grateful to P. Bousquet and P. Peylin for providing us with their atmospheric CO_2 inversion results for the North Atlantic. Supported by NSF grants OCE-0097337 (N.G.) and OCE-0083918 (C.D.K.) and by grants from the NSF and NOAA (N.R.B.).

Supporting Online Material
www.sciencemag.org/cgi/content/full/298/5602/2374/DC1
 Materials and Methods
 Table S1
 References and Notes

7 August 2002; accepted 13 November 2002

Control of Facial Muscle Development by MyoR and Capsulin

Jian-rong Lu,¹ Rhonda Bassel-Duby,¹ April Hawkins,¹ Priscilla Chang,¹ Renee Valdez,¹ Hai Wu,¹ Lin Gan,⁴ John M. Shelton,² James A. Richardson,^{1,3} Eric N. Olson^{1*}

Members of the MyoD family of basic helix-loop-helix (bHLH) transcription factors control the formation of all skeletal muscles in vertebrates, but little is known of the molecules or mechanisms that confer unique identities to different types of skeletal muscles. MyoR and capsulin are related bHLH transcription factors expressed in specific facial muscle precursors. We show that specific facial muscles are missing in mice lacking both *MyoR* and *capsulin*, reflecting the absence of MyoD family gene expression and ablation of the corresponding myogenic lineages. These findings identify *MyoR* and *capsulin* as unique transcription factors for the development of specific head muscles.

The myogenic bHLH transcription factors—MyoD, Myf5, myogenin, and MRF4—control vertebrate skeletal muscle development (1). *MyoD* and *Myf5* act redundantly as myoblast specification genes (2), whereas *myogenin* is required for myoblast differentiation (3, 4). *MyoD* and *MRF4* also play redundant roles in muscle differentiation (5). Although these myogenic genes control a developmental program shared by all skeletal muscles, there is evidence that muscles in the head and trunk differ with respect to the early steps in myogenic lineage specification (6). For example, in *Myf5*^{-/-}*Pax-3*^{-/-} double-mutant mice, the trunk musculature is eliminated, but head muscles are unaffected (7). The devel-

opmental control genes responsible for head muscle formation are unknown.

All skeletal muscle posterior to the head is derived from paraxial mesoderm that becomes segmented into somites (1, 8). In contrast, head muscles are derived from multiple cell lineages, including prechordal mesoderm anterior to the first somite and paraxial mesodermal precursors that migrate into the branchial arches (9–11). MyoR/musculin and capsulin/Pod-1/epicardin are related bHLH proteins transiently expressed in migratory paraxial mesodermal cells in the branchial arches that appear to represent precursors of the muscles of mastication (12–18).

A null mutation in the mouse *capsulin* gene results in neonatal lethality due to pulmonary hypoplasia, but no overt skeletal muscle abnormalities (18, 19). We combined mutations in *MyoR* and *capsulin* to see if there were shared activities or effects not revealed with either single-gene deletion. The *MyoR* gene was targeted in embryonic stem (ES) cells by homologous recombination (fig. S1A). ES cell clones

¹Department of Molecular Biology, ²Department of Internal Medicine, and ³Department of Pathology, The University of Texas Southwestern Medical Center at Dallas, 6000 Harry Hines Boulevard, Dallas, TX 75390–9148, USA. ⁴Center for Aging and Developmental Biology, University of Rochester, Rochester, NY 14642, USA

*To whom correspondence should be addressed. E-mail: eolson@hamon.swmed.edu

REPORTS

harboring the mutant allele were used to generate chimeric mice, which transmitted the mutation through the germ line (fig. S1B). Breeding of mice heterozygous for the mutant *MyoR* allele yielded homozygous mu-

tants at predicted Mendelian ratios with no obvious abnormalities.

Mice homozygous for the *MyoR* and *capsulin* null mutations were obtained by breeding heterozygous mutant mice. Double mu-

tants were born alive, but, like *capsulin*^{-/-} mice (18, 19), they died within minutes after birth. Histological examination revealed a complete absence of the major muscles of mastication, including the masseter, medial and lateral pterygoids, and temporalis muscles in the majority of double-mutant embryos (Fig. 1, A to E). In their place was connective tissue. In a subset of double mutants, atrophic pterygoid myofibers persisted unilaterally. The missing muscles in *MyoR*^{-/-capsulin}^{-/-} double-mutant mice are derived from the first branchial arch and represent a distinct group of muscles that function in mastication (8). Other first arch-derived muscles, such as the anterior digastric and mylohyoid, which do not function in mastication, were present in the double mutants [Fig. 1, A to D and (20)]. Trunk muscles of double mutants were also indistinguishable from those of wild-type animals (20). Head muscle defects were not observed in *MyoR*^{+/-capsulin}^{-/-} or in *MyoR*^{-/-capsulin}^{+/-} embryos. These findings demonstrated that *MyoR* and *capsulin* redundantly controlled the formation of a specific subset of first arch-derived facial skeletal muscles and that a single copy of either gene is sufficient to support normal muscle development.

MyoR^{-/-capsulin}^{-/-} double mutants also displayed cleft palate (Fig. 1C). Other branchial arch-derived skeletal elements were normal in double mutants [Fig. 1 and (20)]. In addition, the visceral organs of *MyoR*^{-/-capsulin}^{-/-} double-mutant neo-

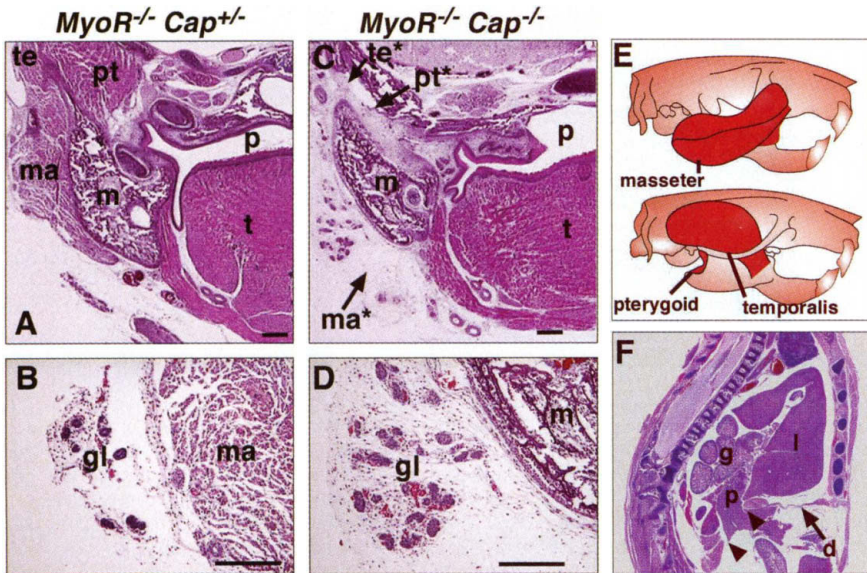


Fig. 1. Deficiency of head skeletal muscle and diaphragmatic hernia in *MyoR*^{-/-capsulin}^{-/-} neonates. Coronal sections from *MyoR*^{-/-capsulin}^{+/-} (A and B) and *MyoR*^{-/-capsulin}^{-/-} (C and D); (B and D) show a higher magnification of (A and C), respectively. Note the cleft palate (p) in (C). gl, glands; m, mandible; ma, masseter muscle; p, palate; pt, pterygoid muscles; t, tongue; te, temporalis muscle. Asterisks in (C) denote missing muscles. In (B), the glands about the masseter, whereas in (D), the masseter is missing and the glands about the mandible. (E) Diagrams of muscle groups missing from the double mutant. (F) Sagittal section of a *MyoR*^{-/-capsulin}^{-/-} with diaphragmatic hernia. Arrowheads mark the boundaries of the diaphragmatic defect. Arrow marks the diaphragm. d, diaphragm; g, gut; l, liver; p, pancreas. Scale bars, 200 μ m.

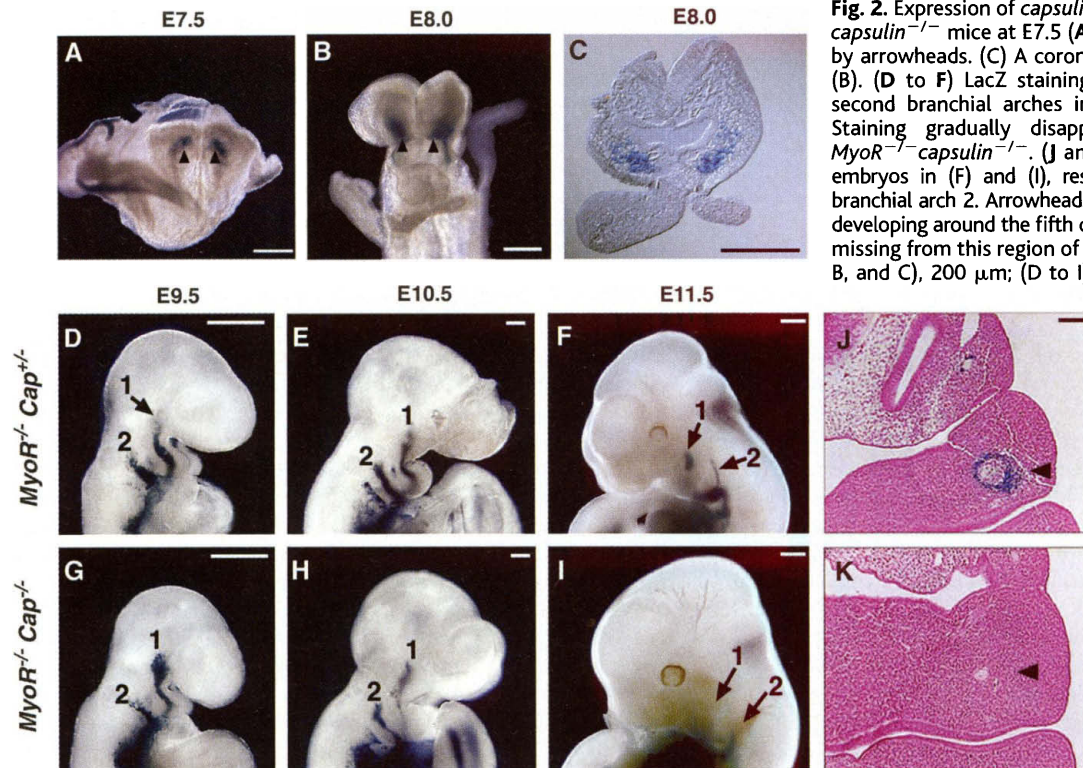


Fig. 2. Expression of *capsulin-lacZ* allele. Expression of lacZ in *capsulin*^{-/-} mice at E7.5 (A) and E8.0 (B and C), as indicated by arrowheads. (C) A coronal section through the embryo in (B). (D to F) LacZ staining is present within the first and second branchial arches in *MyoR*^{-/-capsulin}^{+/-}. (G to I) Staining gradually disappears from the first arch of *MyoR*^{-/-capsulin}^{-/-}. (J and K) Sections of the first arch of embryos in (F) and (I), respectively. 1, branchial arch 1; 2, branchial arch 2. Arrowheads in (J) and (K) indicate the muscle developing around the fifth cranial nerve. LacZ-positive cells are missing from this region of the double mutant. Scale bars: (A, B, and C), 200 μ m; (D to I), 500 μ m; (J and K), 100 μ m.

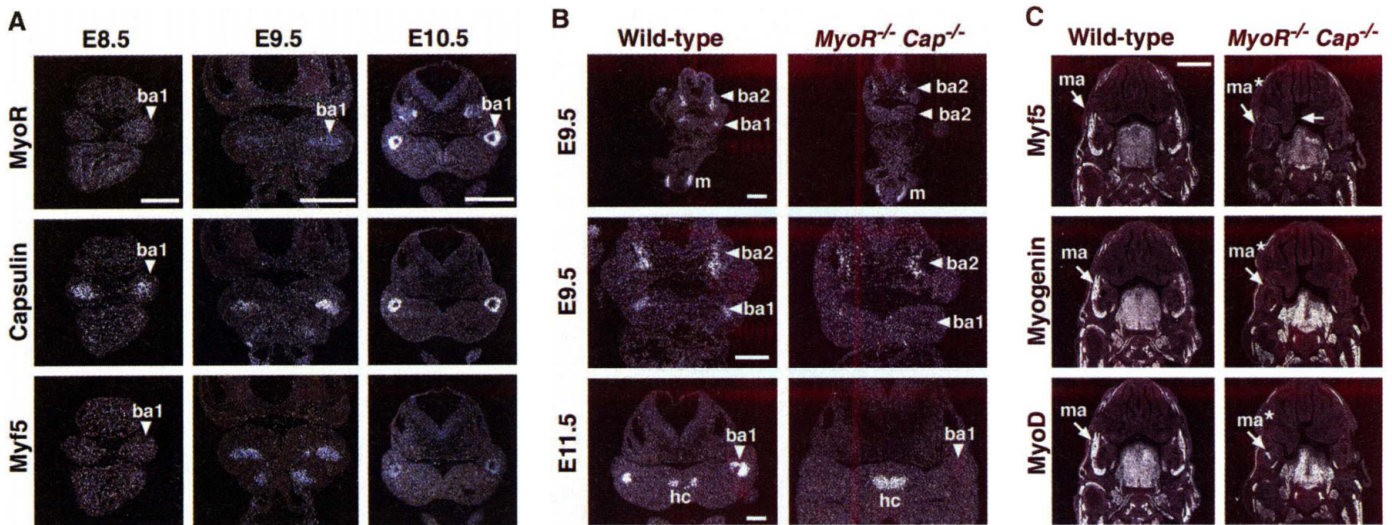


Fig. 3. Expression of myogenic bHLH genes in wild-type and *MyoR*^{-/-}*capsulin*^{-/-} embryos. (A) *MyoR*, *capsulin*, and *Myf5* expression were detected in the branchial arches of wild-type embryos by in situ hybridization. *Capsulin* was detected at E8.5 in the first arch (ba1). Expression of *Myf5* and *MyoR* overlapped that of *capsulin* at later stages. (B) *Myf5* expression was detected in the first branchial arches of *MyoR*^{+/+}*capsulin*^{+/+}, designated wild type, but not in *MyoR*^{-/-}

capsulin^{-/-} embryos. The middle panels show higher magnification of the upper panels. ba1, first branchial arch; ba2, second branchial arch; hc, hypoglossal cord. m, Myotome. (C) *Myf5*, *myogenin*, and *MyoD* expression was detected in wild-type and *MyoR*^{-/-}*capsulin*^{-/-} embryos at E15.5. The masseter muscle (ma) is completely absent in *MyoR*^{-/-}*capsulin*^{-/-} mutants (designated ma*). Arrow indicates cleft palate. Scale bars: 200 μm for (A and B), 1 mm for (C).

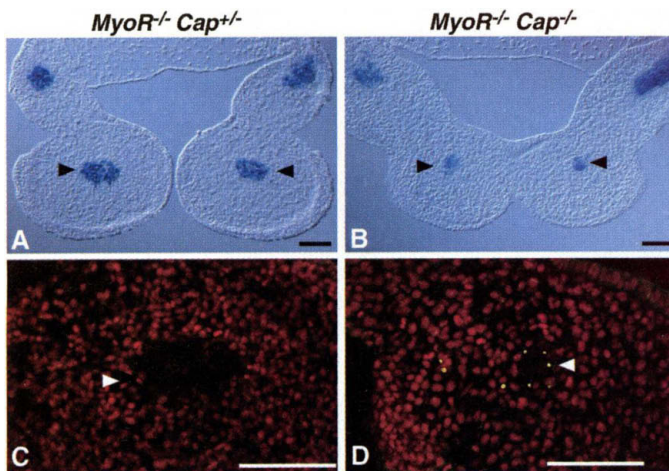


Fig. 4. Apoptosis of muscle cells in the first branchial arch in *MyoR*^{-/-}*capsulin*^{-/-} embryos. First branchial arch of *MyoR*^{-/-}*capsulin*^{+/+} and *MyoR*^{-/-}*capsulin*^{-/-} embryos at E10.5 stained for lacZ expression and viewed by differential interference contrast microscopy. (A and B). The same sections were stained with propidium iodide, and apoptotic cells were identified by TUNEL labeling (C and D). At this stage, lacZ-positive cells are disappearing from the first branchial arch

arches of wild-type and double-mutant embryos (Fig. 2, D and G). By E10.5, a swathe of lacZ-positive cells extended into the first and second branchial arches. This myogenic precursor pool appeared to migrate properly, but there were noticeably fewer of these lacZ-positive cells in the first branchial arch of the double mutants (Fig. 2, E and H). In contrast, other embryonic sites of lacZ expression showed similar staining in embryos of the different genotypes. At E11.5, lacZ expression was observed in presumptive myoblasts within the first and second branchial arches of normal embryos (Fig. 2F). These lacZ-positive cells within the first branchial arch surrounded the fifth cranial nerve (Fig. 2J). There was a dramatic reduction of lacZ staining in the myogenic cores of the first branchial arches of double mutants at E11.5 (Fig. 2, I and K), suggesting that the *capsulin*-expressing myogenic lineage of the first branchial arch was specifically affected in these mutant embryos.

of the double mutant because of apoptosis, as revealed by TUNEL labeling (yellow) in the lacZ-positive cores. LacZ staining interferes with detection of propidium iodide. Arrowheads point to lacZ-positive cores in the first branchial arches. Scale bar, 100 μm.

The striking lack of specific facial skeletal muscles in *MyoR*^{-/-}*capsulin*^{-/-} double mutants was reminiscent of the phenotype associated with the combined absence of *Myf5* and *MyoD*, except that the latter phenotype affects all skeletal muscles (2). To define the temporal sequence of expression of these genes and to determine whether myogenic bHLH genes were expressed in the affected muscle lineage of the double mutant, we performed in situ hybridization with adjacent sections of staged embryos between E8.5 and 15.5. *Capsulin* transcripts were detected in mesodermal precursors of the first arch at E8.5 (Fig. 3A). At this stage, *Myf5*, *MyoD*, and *MyoR* ex-

presses were displaced into the chest through a defect in the posterior region of the diaphragm (Fig. 1F). This abnormality suggests that *MyoR* and *capsulin* are required to maintain integrity of the diaphragm muscle. The diaphragm develops from fusion of the septum transversum, the pleuroperitoneal membrane, and the dorsal esophageal mesentery and is populated by muscle precursor cells that migrate from the cervical somites (21). *MyoR* is expressed in diaphragmatic myoblasts (12, 13), and *capsulin* is expressed in the septum transversum and the pleuroperitoneal membrane (14–18).

The head muscle deficiency in *MyoR*^{-/-}*capsulin*^{-/-} double mutants could arise from a

defect in specification, migration, or proliferation of the affected myogenic lineages; a block in myoblast differentiation; or an increase in apoptosis. To determine the basis for this muscle deficit and to pinpoint the time of its onset, we compared the expression of a lacZ reporter integrated into the targeted *capsulin* allele in staged embryos of the different genotypes. From embryonic day 7.5 (E7.5) to E8.0, when mesodermal precursors of first arch muscle cells initially appear subjacent to the metencephalon (10), lacZ staining was localized to this muscle precursor population in embryos of the different genotypes (Fig. 2, A to C). At E9.5, these lacZ-positive cells could be seen migrating into the newly formed branchial

pression was undetectable. There has been some disagreement about the timing of expression of *Myf5* and *MyoD* in the branchial arches, depending on the method of detection, but the earliest reported expression of these genes in this region is E9.25 and E9.5, respectively (22–24). By E9.5, *Myf5* and *capsulin* were expressed in the same cell population within the first branchial arch, and by E10.5, *Myf5*, *capsulin*, and *MyoR* were coexpressed in these cells of wild-type embryos (Fig. 3A). In contrast, *Myf5* was not expressed in first branchial arch precursors of *MyoR*^{-/-}*capsulin*^{-/-} double mutants at E9.5 or E11.5 (Fig. 3B). There was also no evidence for expression of *Myf5*, *MyoD*, or *myogenin* at E15.5 in the region of affected facial muscles (Fig. 3C), whereas these genes were expressed in other developing head and trunk muscles.

To determine the fate of first arch muscle precursors that failed to activate expression of *Myf5* and *MyoD*, we performed TUNEL (terminal deoxynucleotidyl transferase-mediated dUTP nick-end labeling) on histological sections of double-mutant embryos at E10.5, when cells marked by expression of *capsulin-lacZ* were disappearing. As shown in Fig. 4, TUNEL-positive cells were observed among the lacZ-positive muscle precursors of double mutants, but not of *MyoR*^{-/-}*capsulin*^{+/-} embryos. We conclude that these cells, which fail to initiate the normal program for muscle development in the double mutant, undergo apoptosis with resulting ablation of muscles of mastication. Similar observations have been made in muscle precursor cells in the limb buds of mice lacking *MyoD* and *myf5* (25).

The absence of specific head muscle cells, as well as markers of the corresponding myogenic lineages, in *MyoR*^{-/-}*capsulin*^{-/-} mutants resembles the effect of *MyoD*^{-/-}*Myf5*^{-/-} double mutations on all skeletal muscles (2) and is distinct from the phenotype of *Myf5*^{-/-}*Pax3*^{-/-} mutants, which exhibit a specific deficiency of trunk skeletal muscles (7). This phenotype also differs from that of *myogenin* mutant mice, in which myoblasts express myogenic bHLH genes, but are unable to differentiate (3, 4). These findings demonstrate that *MyoR* and *capsulin* redundantly regulate an initial step in the specification of a specific subset of facial skeletal muscle lineages and that, in the absence of these factors, myogenic bHLH genes are not switched on, and cells from these lineages undergo programmed cell death. There may also be a modest effect on migration of precursors, as is seen in *Lbx1* mutant mice (21). *MyoR* and *capsulin* act as transcriptional repressors in transfection assays (12, 20). Whether they act to repress an inhibitor of myogenesis or have a transcriptional-

activating function during development of facial muscle remains to be determined. The phenotype of *MyoR*^{-/-}*capsulin*^{-/-} mutant mice reveals a previously unanticipated complexity in the development of head skeletal muscles, and these findings identify *MyoR* and *capsulin* as unique transcriptional regulators for the development of specific head muscles.

References and Notes

1. M. Buckingham. *Curr. Opin. Genet. Dev.* **11**, 440 (2001).
2. M. A. Rudnicki et al., *Cell* **75**, 1351 (1993).
3. P. Hastly et al., *Nature* **364**, 501 (1993).
4. Y. Nabeshima et al., *Nature* **364**, 532 (1993).
5. A. Rawls, M. R. Valdez, W. Zhang, J. Richardson, W. H. Klein, E. N. Olson. *Development* **125**, 2349 (1998).
6. A. Rawls, E. N. Olson, *Cell* **89**, 5 (1997).
7. S. Tajbakhsh, D. Rocancourt, G. Cossu, M. Buckingham, *Cell* **89**, 127 (1997).
8. B. Christ, C. P. Ordahl, *Anat. Embryol. (Berlin)* **191**, 381 (1995).
9. D. M. Noden, *Am. J. Anat.* **168**, 257 (1983).
10. P. A. Trainor, S. S. Tan, P. P. Tam, *Development* **120**, 2397 (1994).
11. A. Hacker, S. Guthrie, *Development* **125**, 3461 (1998).
12. J. Lu, R. Webb, J. A. Richardson, E. N. Olson, *Proc. Natl. Acad. Sci. U.S.A.* **96**, 552 (1999).
13. L. Robb, L. Hartley, C. C. Wang, R. P. Harvey, C. G. Begley, *Mech. Dev.* **76**, 197 (1998).

14. J. Lu, J. A. Richardson, E. N. Olson, *Mech. Dev.* **73**, 23 (1998).
15. H. Hidai, R. Bardales, R. Goodwin, T. Quertermous, E. E. Quertermous, *Mech. Dev.* **73**, 33 (1998).
16. S. E. Quaggin et al., *Development* **126**, 5771 (1999).
17. L. Robb et al., *Dev. Dyn.* **213**, 105 (1998).
18. J. Lu et al., *Proc. Natl. Acad. Sci. U.S.A.* **97**, 9525 (2000).
19. S. E. Quaggin et al., *Development* **126**, 5771 (1999).
20. J. Lu, E. N. Olson, unpublished results.
21. H. Brohmann, K. Jagla, C. Birchmeier, *Development* **127**, 437 (2000).
22. M. O. Ott, E. Bober, G. Lyons, H. Arnold, M. Buckingham, *Development* **111**, 1097 (1991).
23. S. Tajbakhsh, E. Bober, C. Babinet, S. Pournin, H. Arnold, M. Buckingham, *Dev. Dyn.* **206**, 291 (1996).
24. J. C. J. Chen, C. M. Love, D. J. Goldhammer. *Dev. Dyn.* **221**, 274 (2001).
25. B. Kablar, K. Krastel, C. Ying, S. J. Tapscott, D. J. Goldhammer, M. A. Rudnicki. *Dev. Biol.* **206**, 21931 (1999).
26. We are grateful to C. Pomajzl and J. Stark for histologic preparations. We also thank A. Tizenor for graphics and J. Page for editorial assistance. Supported by grants from the NIH, the Donald W. Reynolds Foundation and the Muscular Dystrophy Association to E.N.O.

Supporting Online Material

www.sciencemag.org/cgi/content/full/298/5602/2378/DC1

Materials and Methods

Fig. S1

References

9 September 2002; accepted 28 October 2002

Genetic Structure of Human Populations

Noah A. Rosenberg,^{1*} Jonathan K. Pritchard,² James L. Weber,³ Howard M. Cann,⁴ Kenneth K. Kidd,⁵ Lev A. Zhivotovskiy,⁶ Marcus W. Feldman⁷

We studied human population structure using genotypes at 377 autosomal microsatellite loci in 1056 individuals from 52 populations. Within-population differences among individuals account for 93 to 95% of genetic variation; differences among major groups constitute only 3 to 5%. Nevertheless, without using prior information about the origins of individuals, we identified six main genetic clusters, five of which correspond to major geographic regions, and subclusters that often correspond to individual populations. General agreement of genetic and predefined populations suggests that self-reported ancestry can facilitate assessments of epidemiological risks but does not obviate the need to use genetic information in genetic association studies.

Most studies of human variation begin by sampling from predefined “populations.” These populations are usually defined on the basis of culture or geography and might not reflect underlying genetic relationships (1). Because knowledge about genetic structure of modern human populations can aid in inference of human evolutionary history, we used the HGDP-CEPH Human Genome Diversity Cell Line Panel (2, 3) to test the correspondence of predefined groups with those inferred from individual multilocus genotypes (supporting online text).

The average proportion of genetic differences between individuals from different human populations only slightly exceeds that

between unrelated individuals from a single population (4–9). That is, the within-population component of genetic variation, estimated here as 93 to 95% (Table 1), accounts for most of human genetic diversity. Perhaps as a result of differences in sampling schemes (10), our estimate is higher than previous estimates from studies of comparable geographic coverage (4–6, 9), one of which also used microsatellite markers (6). This overall similarity of human populations is also evident in the geographically widespread nature of most alleles (fig. S1). Of 4199 alleles present more than once in the sample, 46.7% appeared in all major regions represented: Africa, Europe, the Middle East, Central/